ChemCatChem

Research Article
doi.org/10.1002/cctc.202200472

Chemistry Europe
European Chemical Societies Publishing

www.chemcatchem.org

Beneficial Effects of Low Iron Contents on Cobalt-Containing Spinel Catalysts in the Gas Phase 2-Propanol Oxidation

Maik Dreyer,[a] Ulrich Hagemann,[b] Markus Heidelmann,[b] Eko Budiyanto,[c] Nicolas Cosanne,[d] Klaus Friedel Ortega,[d] Sharif Najafishirtari,[d] Nils Hartmann,[b] Harun Tüysüz,[c] and Malte Behrens*[a, d]

Oxidation reactions are highly relevant transformation reactions in the industry. Mixed Co and Fe containing oxides are promising substituents for noble-metal-based catalysts due to lower cost and higher thermal stability. Performing oxidation catalysis in the liquid phase is desired to prevent total oxidation. An approach toward liquid phase reactions is water vapor added to the gas stream, which can help to build an experimental bridge between both phases. Here, nanocasted $Co_{3-x}Fe_xO_4$ spinels are studied in the gas phase oxidation of 2-propanol as a probe for selective oxidation without and with the addition of water into the reaction feed. In both cases, low amounts of Fe ($\leq$4%) were found to be beneficial for the activity. Under wet conditions, there is a negative effect on the activity below 150 °C during heating due to competitive adsorption. However, at higher temperatures during cooling, the activity is higher due to a slower deactivation.

Introduction

Cobalt-containing spinel oxides are among the most promising materials studied in recent years to replace noble-metal-based catalysts in oxidation catalysis for the formation of value-added products or in total oxidation processes.[1] Thus, the oxidation reactions of several reactants were extensively studied on cobalt-based spinel catalysts, such as CO oxidation,[2] methane combustion,[3] longer-chain alkane combustion,[4] as well as gas phase and liquid phase 2-propanol oxidation.[5]

From the mechanistic point of view, the O_2 activation and the formation of reactive oxygen species (ROS) at the surface of these cobalt oxide catalysts play an important role in CO and methane oxidation.[6] Zasada et al. reported that two fivefold coordinated Co^{3+} centers in octahedral sites of the spinel activate the oxygen as a cooperative tandem.[7] In the temperature range below 450 °C, they reported μ-superoxo and metal-oxo species.[3b] Another study by Liu et al. showed that oxygen vacancies could activate O_2 and form superoxo species on the surface.[8] In general, cobalt oxide spinel with a predominantly exposed (110) surface shows higher activity than that of materials with other low-indexed surface terminations as seen in CO oxidation,[2e] gas-phase 2-propanol oxidation,[5a] methane,[9] and toluene oxidation.[10] CO oxidation is considered to take place by different mechanisms. The mechanisms mentioned by Lukashuk et al. are namely Langmuir-Hinshelwood at low temperature, Mars-van-Krevelen at high temperature, and the additional mechanisms CO dissociation, carbon oxidation, and formation of carbonate spectators.[11]

2-Propanol oxidation on Co_3O_4 spinel catalysts was mainly studied as a probe reaction for selective oxidations relevant to the chemical industry. It was proposed that coordinatively unsaturated Co^{3+} is the active site in the liquid- and gas-phase oxidation.[5c,e] In terms of 2-propanol oxidation on the (100) surface, a preferential Langmuir-Hinshelwood mechanism was reported,[5c] while on the (110) surface, the Mars-van-Krevelen mechanism was proposed based on DFT + U calculations.[5a]

On spinel oxides, the addition of water to the reaction feed typically dampens the activity in oxidation catalysis,[12] which was observed on Co_3O_4-based spinel catalysts in several reactions under wet conditions, e.g., total propane oxidation,[4a] hydrocarbon oxidation,[12] and CO oxidation.[13] The lower CO oxidation activity was related to water adsorption on Co^{3+} sites. Consequently, the sites are not available for the adsorption of reactant molecules.[13] Another possible reason is surface coverage with OH groups instead of H_2O[13] which possibly hinders

[a] M. Dreyer, Prof. M. Behrens
Faculty for Chemistry and Center for Nanointegration Duisburg-Essen (CENIDE), University of Duisburg-Essen
Universitätsstr. 7
D-45141 Essen (Germany)
E-mail: mbehrens@ac.uni-kiel.de
[b] Dr. U. Hagemann, Dr. M. Heidelmann, Prof. N. Hartmann
Interdisciplinary Center for Analytics on the Nanoscale (ICAN), and Center for Nanointegration Duisburg-Essen (CENIDE), NanoEnergieTechnikZentrum at University of Duisburg-Essen
Carl-Benz-Str. 199
D-47057 Duisburg (Germany)
[c] E. Budiyanto, Dr. H. Tüysüz
Heterogeneous Catalysis and Sustainable Energy
Kaiser-Wilhelm-Platz 1
D-45740 Mülheim an der Ruhr (Germany)
[d] N. Cosanne, Dr. K. F. Ortega, Dr. S. Najafishirtari, Prof. M. Behrens
Institute of Inorganic Chemistry,
Christian-Albrechts-Universität zu Kiel
Max-Eyth-Straße 2
D-24118 Kiel (Germany)

Supporting information for this article is available on the WWW under https://doi.org/10.1002/cctc.202200472

the oxygen transfer.[13–14] However, a different reaction mechanism occurs on the (110) surface; a CO molecule can additionally be adsorbed on a Co^{3+} with a pre-adsorbed OH group and still form CO_2.[13] Our previous work showed a lower deactivation rate in a wet feed than a dry feed on cobalt iron mixed perovskites,[15] which shows that also positive effects of water addition are possible, that need further studies.

A general synergistic effect of different cations was reported in the literature for several reactions regarding the catalyst composition. For example, the highest selectivity to lower olefins in CO hydrogenation was found for an intermediate Mn content in $Mn_xFe_{3-x}O_4$ spinels.[16] The same was observed for the activity of $Mn_xZn_{1-x}Fe_2O_4$ materials in the gas-phase oxidation of benzyl alcohol.[17] In N_2O decomposition, Wójcik et al. showed the effects of doping with various cations, where surface promotors like Na, K, and Cs had a beneficial effect on the catalytic activity with content of <1.5 wt.%, whereas positive effects of bulk substituents Ni and Zn were achieved with contents of 17 and 11 wt.%, respectively.[18] Also, a beneficial effect of Fe was reported previously in the literature when doping Mn_3O_4 spinel catalysts in the reduction of NO with ammonia, attributed to a Fe_{oct}-O-Mn_{tet} site.[19] Also, in the electrocatalytic oxygen evolution reaction (OER), the doping effects of Fe on Co_3O_4 are extensively reported in the literature.[20] As a result of DFT+U calculations, a beneficial effect of Fe doping at an octahedral site on a Co_3O_4(001) A-layer with exposed tetrahedrally coordinated Co was found to lower the overpotential of the reaction.[21]

Iron substitution in the Co_3O_4 spinel catalyst was studied on mesoporous materials synthesized via the nanocasting method using SBA-15 silica as a hard-template. An increase of catalytic activity in cinnamyl alcohol oxidation in the liquid phase catalyzed by these catalysts was observed when *tert*-butyl hydroperoxide (TPHP) was used as the oxidant. In contrast, no beneficial effect was seen in cinnamyl alcohol oxidation with O_2 as the oxidant.[22] A similar catalytic enhancement promoted by iron substitution could also be observed in cinnamyl alcohol oxidation reaction with TBHP oxidant and $LaCo_{1-x}CoFe_xO_3$ perovskite catalysts.[23] In the electrochemical OER catalyzed by the aforementioned SBA-15 templated spinels, iron substitution could facilitate a faster reaction kinetics due to the higher spin state of Co^{3+} ions in octahedral positions,[5c,24] and alteration in the Co^{3+}-O bonds.[20a]

In this study, effects of water addition and iron doping/incorporation are investigated for 2-propanol oxidation using empirical composition-activity correlations in dry and wet feeds. The catalysts are mixed mesoporous $Co_{3-x}Fe_xO_4$ spinel catalysts, synthesized using SBA-15 silica hard template via the nanocasting route as described in the literature.[5e,20a,22] The composition of the samples was varied in a range from a few percent of Fe substitution in Co_3O_4 to $CoFe_2O_4$ and they were characterized by powder X-ray diffraction (XRD), X-ray photoelectron spectroscopy (XPS), high-resolution scanning transmission electron microscopy (STEM), electron energy loss spectroscopy (EELS) and energy-dispersive X-ray spectroscopy (EDX). After thorough characterization, the materials were tested in the gas phase oxidation of 2-propanol in three consecutive runs. Before each run, temperature-programmed oxidation (TPO) was performed to restore the catalysts' initial conditions. The first two runs were performed without a co-feed of water into the gas stream. A tenfold amount of water was added to the feed for the 3rd run. In both cases, a non-stable but highly active low-temperature (LT) activity channel and a less active but stable high-temperature (HT) activity channel were observed. Under both dry and wet conditions, a beneficial effect of small contents of Fe (≤ 4%) was seen. On the LT activity, the effect of water is always detrimental. However, when cooling down, water has a beneficial effect that coincides with higher stability during an isothermal dwell at 300 °C. Post-mortem characterization reveals morphologic stability of the hard templated catalysts and no clear connection between Co content and surface-near Co oxidation state changes.

Results and Discussion

Characterization

The synthesis and characterization of SBA-15 templated cobalt iron oxide ($Co_{3-x}Fe_xO_4$) sample series with the Co:Fe atomic ratios of 100:0 (Co_3O_4), 64:1, 32:1, 16:1, 7:1, 3:1, and 1:2 ($CoFe_2O_4$) were reported in detail in previous publications and are summarized in the following paragraph.[5e,20a, 22] The above-mentioned ratios refer to the nominal stoichiometric ratio of Co:Fe used in the synthesis, and the composition was verified by scanning transmission electron microscopy (STEM) energy-dispersive X-ray spectroscopy (EDX) and X-ray photoelectron spectroscopy (XPS). XRD analysis revealed a pure single spinel phase on Co_3O_4 and $Co_{3-x}Fe_xO_4$ with Co:Fe atomic ratios of 64:1, 32:1, 16:1. For mixed samples with Co:Fe ratios of 7:1, 3:1 and 1:2 the two miscible phases of Co_3O_4 and $CoFe_2O_4$ could be assigned.[5e] With increasing Fe content in the catalysts, transmission electron microscopy (TEM) revealed less ordering of the mesoporous structure and nanowire length, as also visible from TEM images before catalysis in this study (see Figure S1). Another effect of incorporating Fe was seen on the increase of occupancy of Co^{2+} species in tetrahedral sites and distorted Co^{3+}-O bonds.[20a] A bulk elemental analysis by STEM-EDX and near-surface elemental quantification by X-ray photoelectron spectroscopy (XPS) showed a good agreement of the experimental Co:Fe content compared to its nominal or theoretical value, as shown in Figure 1a.[5e,22] The Co 2p XPS spectra of the as-prepared materials are shown in Figure S2. The results for the STEM-EDX and XPS analysis are given in Table 1.

Comparing STEM-EDX and XPS, a considerable difference in Co content on the surface compared to the bulk was seen only for the $CoFe_2O_4$ catalyst. A greater extent of Co in the near-surface regions was also reported before for the SBA-15 templated $CoFe_2O_4$ catalyst, which might be in line with the confirmation of a surface-segregated Co_3O_4 secondary phase in this sample, as shown by Rietveld refinement.[5e,22] The evaluation of Co species was then performed with XPS spectra. In general, fitting the Co 2p region is prone to errors in mixed Co

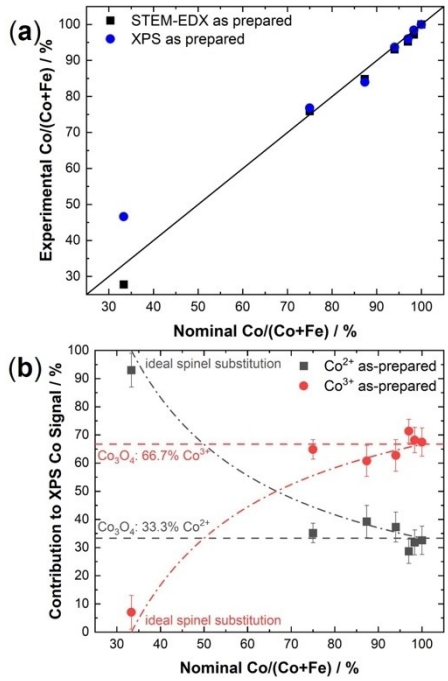

Figure 1. (a) Parity plot of experimental Co/(Co + Fe) ratio derived from STEM-EDX and XPS in the as-prepared state. (b) Contribution of Co^{2+} and Co^{3+} to the Co XPS signal in the as-prepared state. The dashed horizontal lines indicate the Co oxidation state composition of a normal Co_3O_4 spinel with 33.3 % Co^{2+} and 66.7 % Co^{3+}. The hyperbole curves show the Co oxidation states when substituting Co by Fe in Co_3O_4 under the assumption that Fe exclusively is present as Fe^{3+}.

and Fe containing oxides.[25] Since Co^{2+}/Co^{3+} oxidation states were desired to be investigated, and not CoO and Co_3O_4 phase contributions, a model using the reference fits of Co^{2+} in CoO from the literature[25a] and Co^{3+} from a measurement on a $MgCo_2O_4$ catalyst synthesized by Rabe et al.[26] was further constructed. For the three samples with the highest Fe contents, the Fe-LMM Auger peak overlapping with the Co 2p peak cannot be neglected. As the Fe is present as Fe^{3+} in our samples, we used the reference spectra from a Fe_2O_3 sample to model the size, shape, and position of the Fe Auger signal. Especially for the $CoFe_2O_4$ sample, this leads to an increase in the precision for the Co species determination. The results are shown in Figure 1b, and only minor changes between the different samples are observed. Two different reference composition curves are given per species. The horizontal curves show the ratio from a normal Co_3O_4 spinel consisting of 2/3 Co^{3+} in octahedral positions and 1/3 Co^{2+} in tetrahedral positions. The hyperboles show the composition upon substitution of Co by Fe under the assumption that Fe is always present as Fe^{3+}, as indicated from the Fe 2p signals. A comparison between data and references reveals that the data mimics the behavior well with the hyperbolic curve shape despite for 3:1, which shows the composition of a normal spinel. For 32:1 and 64:1, the values determined by XPS are slightly higher than expected by both methods. For $CoFe_2O_4$, expected as an inverse spinel with only Co^{2+} contributions, minor contributions of a Co^{3+} species are possible, which is in line with phase segregation reported in the literature.[5e]

In electron energy loss spectroscopy (EELS), the Co L_3/L_2 intensity ratio was determined from spectra shown in Figure S3a and the calculated ratio is shown in Figure S3b for all catalysts. A higher value of this ratio indicates a lower oxidation state of the Co cations.[27] This local spectroscopy technique confirmed that all catalysts despite $CoFe_2O_4$ show comparable Co oxidation states and that $CoFe_2O_4$ has a lower overall Co oxidation state. Furthermore, it is confirmed that the catalyst 3:1 differs from the expected hyperbole curve (Figure 1b) assuming a static Fe^{3+} oxidation state.

Specific BET surface areas of the catalysts are reproduced from the previous work[6] with the exception of Co:Fe 64:1 and are shown in Table 1. For Co-rich samples, the exposed surface areas ranged between 103 and 128 $m^2 g^{-1}$. For $CoFe_2O_4$, the surface area increased to 178 $m^2 g^{-1}$ due to the formation of small nanoparticles instead of elongated nanowires arrays.[20a]

Catalysis data evaluation procedure

As previously applied in a study of $LaFe_{1-x}Co_xO_3$ perovskites,[15] a consecutive three-run catalytic procedure was used to determine the activity of the catalyst materials in the gas phase oxidation of 2-propanol as a function of Co content in the catalyst as well as of the water content in the reaction mixture. Each run consisted of heating and cooling segments separated by an isothermal dwell period of 1 h at 300 °C. The two first runs were performed in a 1:1 mixture of O_2 and 2-propanol under identical conditions to check for stability and performance restorability. The 3rd run was performed with the 10-fold co-dosing of water compared to 2-propanol and O_2 into the feed to study its effect compared to the dry runs. Before each

Table 1. BET surface areas from Ref. [1] and experimental Co/(Co + Fe) ratios determined by the catalysts' STEM-EDX and XPS.

Sample	SA_{BET}	Co/(Co + Fe) [%]		
	[$m^2 g^{-1}$]	Nominal	EDX	XPS
Co_3O_4	107[66]	100.0	100.0	100.0
Co:Fe 64:1	128	98.5	97.2	98.4
Co:Fe 32:1	118[6]	96.9	95.2	96.0
Co:Fe 16:1	103[6]	94.1	93.1	93.7
Co:Fe 7:1	113[6]	87.5	84.8	84.0
Co:Fe 3:1	125[6]	75.0	75.9	76.8
$CoFe_2O_4$	178[6]	33.3	27.8	46.6

catalytic run, an oxidative treatment was performed to burn off surface-blocking carbonaceous species and regenerate the catalyst's surface. This oxidative activation step could fully restore the conversion profile for all catalysts. For the Co_3O_4 catalyst, the steady-state conversion was comparable to that observed during cooling in the transient experiment.[5e] Such comparable conversions during cooling and under steady-state conditions were also observed in the gas-phase 2-propanol oxidation on perovskites.[15]

In Figure 2, an exemplary dataset is shown for Co:Fe 64:1. In the 1st and 2nd runs, the typical pattern of spinel catalysts was observed with a low-temperature (LT) conversion maximum during heating, which disappeared during cooling. Still, it can be restored after temperature-programmed oxidation between the 1st and 2nd run.[5a–d] The behavior of the LT and its disappearance during cooling were explained in a previous study[5d] and it was ascribed to reversible surface poisoning by acetate species and, to a lesser degree, to reduction of Co^{3+} to Co^{2+} on the catalyst surface. Because of this, a local maximum and drop of conversion can be observed for spinel and perovskite catalysts. The calculated carbon balances, which are shown in Figure S4, of our conversions support this claim. Until the temperature reached 130 °C, the only products are acetone coupled with water, indicating an oxidative dehydrogenation pathway. CO_2 evolution from total oxidation is observed at higher temperatures, accompanied by a decrease in acetone yield in the high-temperature (HT) channel. The restorability of the conversion curves in the 1st and 2nd run is shown for all catalysts in Figure S5 with very similar profiles. Therefore, further detailed evaluations in the following discussion are based only on the 1st run.

When co-feeding water in the 3rd run, the conversion curves show the same general features of LT and HT reaction channels, but changes in the catalytic profiles are observed and discussed in detail below. Therefore, the activity of the catalysts was compared based on reactivity parameters,[15] which are graphically shown in Figure 2 with the example of Co:Fe 64:1. Furthermore, the LT reaction channel is characterized by two factors: the temperature needed to reach 10% conversion (T_{10}) during heating and the surface-area normalized 2-propanol consumption rate at 100 °C. On the other hand, the HT channel is characterized by T_{10} and T_{50} during cooling and the reaction rate at 200 °C during cooling. In terms of product formation, oxidative dehydrogenation to acetone remains the main reaction pathway in the wet feed. At the same time, the onset of the CO_2 formation shifts to higher temperatures, and the drop in acetone formation at high temperatures is less pronounced than in the dry feed indicating an additional effect of water on the selectivity.

Effect of Fe doping and substitution on gas phase 2-propanol oxidation activity

2-Propanol conversion curves are shown in Figure 3a for all catalysts. The typical features like the unstable LT activity channel are present in the conversion curves of all different catalyst materials during heating, which is discussed in more detail in the Supporting Information (SI) pages S6 and S7. Corresponding O_2 conversions with similar trends as 2-propanol are shown in Figure S5g and the product distributions are depicted in Figure S6.

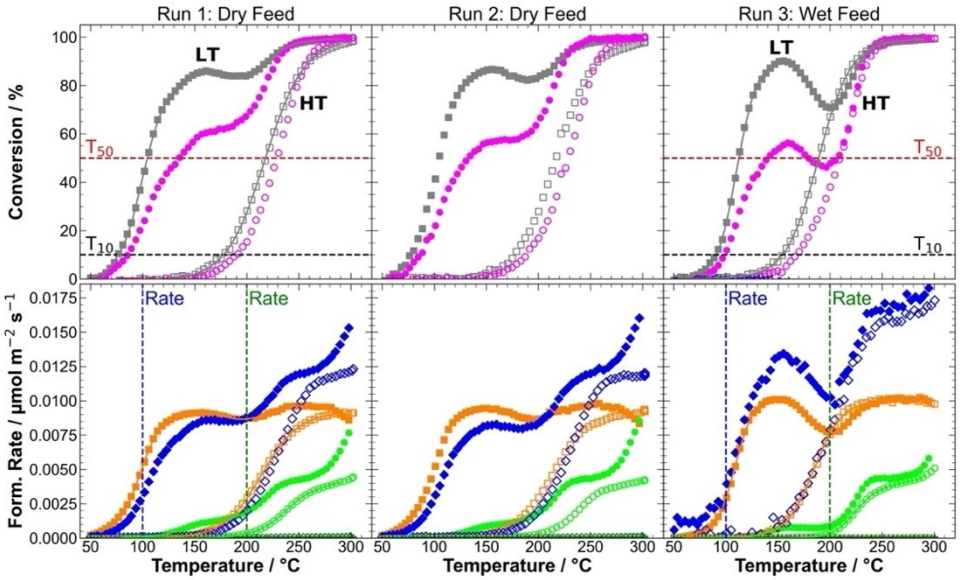

Figure 2. Exemplary dataset of Co:Fe 64:1 obtained from gas phase 2-propanol oxidation consisting of conversions of 2-propanol (■) and oxygen (●, top row) and product formation rates for acetone (■), water (◀) and CO_2 (●, bottom row) during three consecutive runs. Filled symbols show data points during heating. Empty characters show the behavior during cooling. Solid lines indicate the fit of the curve. Parameters T_{10}, T_{50}, and the reaction rates at 100 °C and 200 °C are shown where they were extracted with dashed lines.

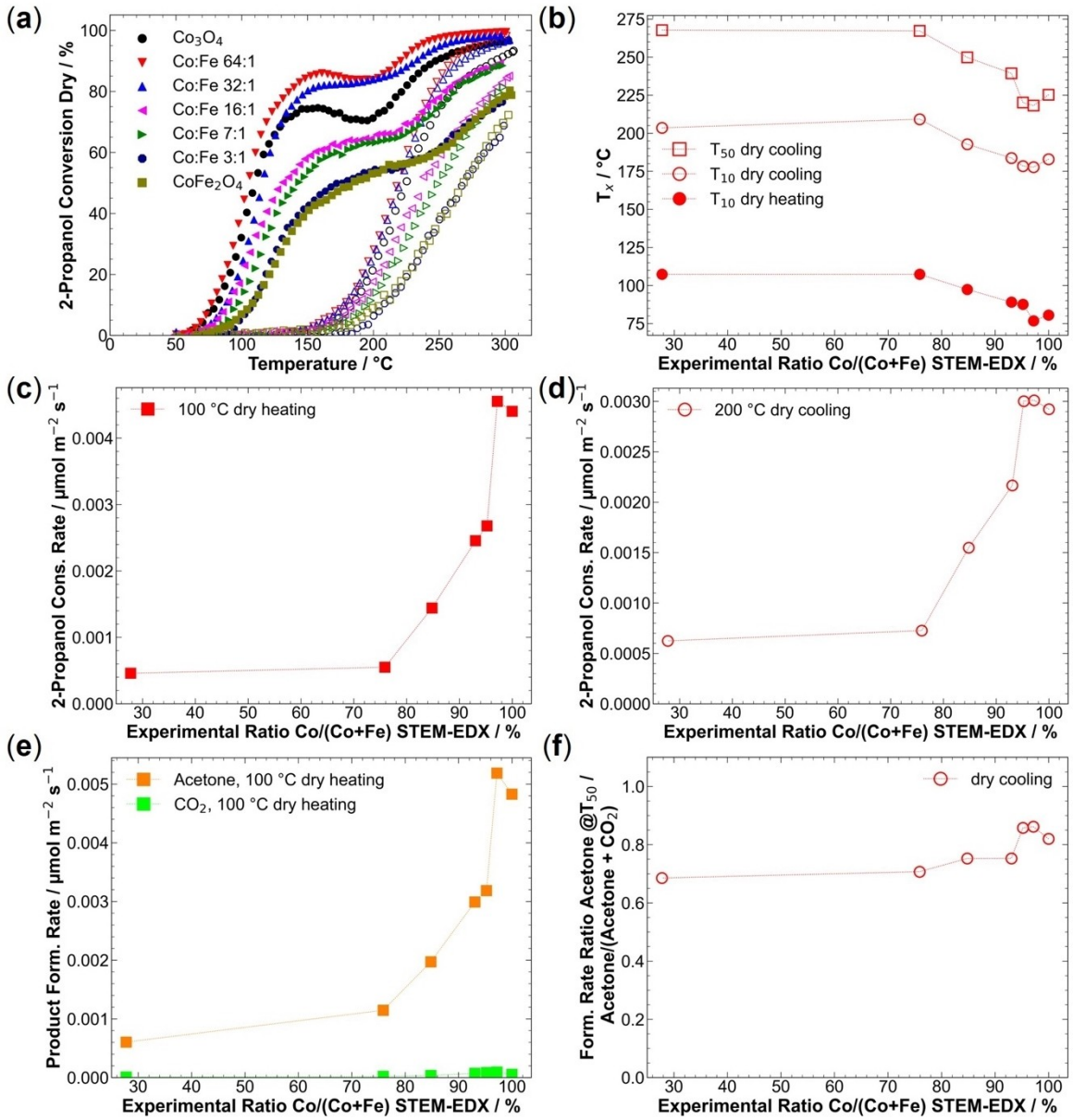

Figure 3. (a) 2-Propanol conversions in dry feed. Solid and hollow symbols show data points during heating and cooling, respectively. (b) T_{10} values during heating and cooling and T_{50} during cooling in dry feed plotted against the experimental Co/(Co + Fe) derived from STEM-EDX. (c) Surface-area normalized 2-propanol consumption rates at 100 °C during dry feed heating. (d) Surface-area normalized 2-propanol consumption rates at 200 °C during dry feed cooling. (e) Surface-area normalized acetone and CO_2 formation rates at 200 °C during cooling. (f) Surface-normalized formation ratio of acetone/(acetone + CO_2) at T_{50} during cooling.

A comparative discussion of the catalytic data is conducted here using the conversion-based reactivity parameters T_x and rates in Figure 3b–f as a function of the experimental cobalt content Co/(Co + Fe) determined by STEM-EDX. The T_{10} values during heating as an indicator for LT channel activity indicate a general decrease of activity with increasing Fe content seen by a higher T_{10} value until the Co:Fe ratio of 3:1 (Figure 3b). After further increasing the Fe content, no further negative effect on this activity parameter was observed. However, there is a small promotion by the smallest amount of Fe incorporated into the catalyst seen by a slightly decreased T_{10} value for Co:Fe 64:1 compared to the pristine Co_3O_4. This coincides with an increase in the specific surface area of Co:Fe 64:1 compared to the pristine Co_3O_4. In the HT channel, represented by T_{10} and T_{50} during cooling, similar trends for both parameters are observed (Figure 3b). Both parameters show a promoting effect of Co:Fe 64:1 and Co:Fe 32:1 with a minimum in the required temperature. The general negative impact of high Fe contents remains present, even though the T_{10} value for Co:Fe 3:1 during cooling indicates less activity than for $CoFe_2O_4$.

After all, variation of the Co content below a Co:Fe ratio of 3:1 in the material was not found to have an apparent effect

on catalytic conversion. In contrast, a trend of increasing activity with a maximum at the Fe doping level was observed for higher Co content. In the liquid phase oxidation of 2-propanol with O_2 as the oxidant and in the CO oxidation, no beneficial effect of doping with small amounts of Fe was found on the similar catalysts presented in this study.[5e,6] In contrast, for CO oxidation, Baidya et al. reported activation of Co_3O_4 catalysts with Fe doping synthesized via solution combustion. This was discussed as an effect of the Fe^{2+}/Fe^{3+} redox couple since TPR showed that the Co^{3+}-O bonding strength is only slightly higher than Fe^{3+}-O.[28]

Since coordinatively unsaturated Co^{3+} in octahedral sites is considered as the active site in 2-propanol oxidation,[5e] especially on 110-oriented spinel surfaces,[5a] a positive effect of the increasing ratio of tetrahedrally to octahedrally coordinated Co species seems no reasonable explanation for the activity increase observed for low Fe contents.[20a] A beneficial effect of Fe was reported previously in the literature when doping Mn_3O_4 spinel catalysts in the reduction of NO with ammonia, attributed to a Fe_{oct}-O-Mn_{tet} site.[19] In the OER, the doping effects of Fe on Co_3O_4 are extensively reported in the literature.[20]

From DFT + *U* calculations, a beneficial effect of Fe doping at an octahedral site on a 001 terminated Co_3O_4 spinel A-layer with exposed tetrahedrally coordinated Co was found to lower the overpotential on the electrochemical OER.[21] Co:Fe 64:1 is more active than Co_3O_4 in terms of T_x but also has a higher specific surface area and much larger pore volume. Furthermore, the $CoFe_2O_4$ catalyst features a higher BET surface area by a factor of 1.7 than the lowest surface area material. Therefore, rates were calculated and normalized based on the exposed surface area. The weight-normalized 2-propanol consumption rates and the specific surface-area normalized rates are shown in Figure S7c and Figure S7e, respectively. Regarding the rate at 100 °C during heating shown in Figure 3c and representing the LT channel, the beneficial effect of doping Co_3O_4 with a low Fe content remains valid, and the maximum rate was detected for this catalyst.

From the 2-propanol consumption rates at 200 °C during cooling, i.e., the kinetic parameter for the HT channel, the beneficial effect of Fe doping was confirmed for Co:Fe 64:1 and Co:Fe 32:1 as well as the detrimental impact of further increasing the Fe content in the catalyst as shown in Figure 3d.

In terms of product formation at 200 °C during cooling, the main products, acetone, and CO_2 are considered for further comparison to investigate the effect of Co content on the product distribution, as shown in Figure 3e. For $CoFe_2O_4$ and Co:Fe 3:1, only minor contents of CO_2 were detected, while for the other catalysts, a notable amount of CO_2 formed and increased with increasing Co content in the spinel materials. The acetone formation rate increased with Co content but showed a maximum at Co:Fe 32:1 and decreased slightly for Co:Fe 64:1 and Co_3O_4. The formation rate ratio acetone/(acetone + CO_2) at T_{50} during cooling (HT channel) is shown in Figure 3f and offers a relatively constant ratio in the range of 70–80% selective oxidation. However, interestingly, Co:Fe 64:1 and Co:Fe 32:1 show a higher ratio of acetone to CO_2 and not only a higher conversion. This indicates that low amounts of Fe promote acetone formation, but not the further total oxidation to CO_2.

In summary, all catalyst materials show a more active but non-stable LT activity channel that disappears after the heating segment with lower catalytic activity on the Fe-rich catalysts. However, the activity does not increase linearly with the Co content. In the LT channel, the presence of a tiny amount of Fe improves the activity compared to the pure Co_3O_4, while in the HT channel, a similar effect is observed on the samples with 1.6–4% of Fe content. In addition, the selectivity towards selective oxidation is increased in these doped catalysts compared to the other samples studied in this substitution series.

Effect of water on the gas phase 2-propanol oxidation activity

Wet feed conversion curves for 2-propanol are shown in Figure 4a and corresponding O_2 conversions in Figure S7h. As discussed in the SI, several more minor differences can be observed in comparing dry and wet feed conversion curves. The product distribution for all catalysts is shown in Figure S6. These and several more minor differences observed in comparing dry and wet feed conversion are discussed in the SI on pages S6 and S7 in more detail and compared to the recent study on perovskites.[15] The differences between dry and wet feed are discussed here based on the aforementioned kinetic parameters and are now newly introduced as the difference between dry and wet feed (Δ) in Figure 4b–f. The ΔT_x values in Figure 4b describe the effect of water in the feed. In this regard, a negative ΔT_x value indicates lower activity in the wet feed, while a positive value indicates a promoting effect of water on the activity. The absolute values for dry and wet are shown in Figure S8a. From the ΔT_{10} value during heating, a clear negative impact of water on the LT activity is seen, as reported previously for perovskites.[15] This shift of the onset of the reaction to higher temperatures can be explained by the competitive adsorption of water on the catalyst surface.[15,29] Consequently, the LT activity observed in the dry feed for increasing Co contents was quenched by the presence of water, and the negative effect became more pronounced. This effect is supported by steady-state data at 160 °C close to the temperature of the LT maximum on Co_3O_4 from a previous study (reproduced and depicted in Figure S9),[5e] where a fast deactivation of the LT channel was observed under dry and wet conditions.

In the HT channel based on ΔT_x during cooling in Figure 4b, except $CoFe_2O_4$, all catalysts are positively affected by the addition of water into the feed gas stream. This beneficial effect increases with increasing Co content in the spinel, although from Co:Fe 32:1 upwards, the effect remains nearly unchanged in ΔT_{50}. Inspection of the absolute values in Figure S8 shows that the promoting effect of low amounts of Fe observed in the dry feed is also present in the wet feed for T_{50}. This observation is also in line with the previous perovskite-based study. The conversion curves during wet cooling were found to shift to

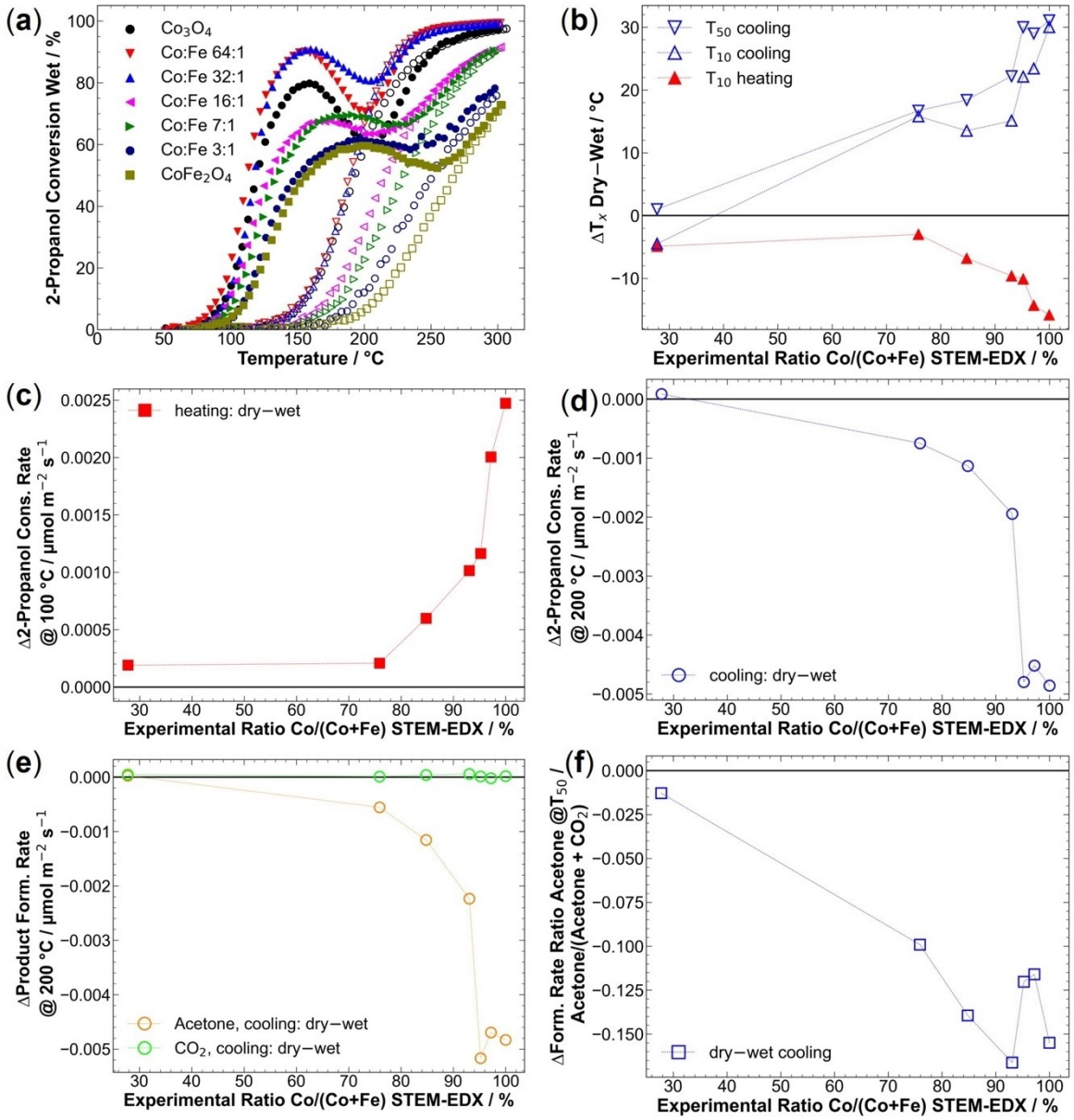

Figure 4. (a) 2-Propanol conversions in wet feed. Solid and hollow symbols show data points during heating and cooling, respectively. (b) Differences between T_{10} during heating cooling and T_{50} during cooling for T_x dry, and T_x wet differences (Δ = dry-wet) plotted against the experimental Co/(Co + Fe) derived from STEM-EDX. (c) Differences between surface-area normalized 2-propanol consumption rate at 150 °C during heating. (d) Surface-area normalized 2-propanol consumption rate differences at 200 °C during cooling. (e) Differences in surface-area normalized acetone and CO_2 formation rates at 200 °C during cooling. (f) The difference in the acetone/(acetone + CO_2) ratio at T_{50} during cooling.

lower temperatures for high Co contents compared to the dry feed on the same catalyst. This was interpreted as a boosted activity of the HT channel or a slower deactivation of the Co-rich catalysts under wet conditions.[15]

In a liquid phase 2-propanol oxidation study by Falk et al. on the same catalytic materials, no beneficial effect of Fe doping on the spinel catalysts was seen, indicating differences between wet feed gas phase and liquid phase catalysis attributed to different active oxygen species in gas- and liquid phase oxidation.[5e] A beneficial effect of Mn doping in Co_3O_4 cubes is reported in the simultaneous oxidations of CO, C_3H_6, and C_3H_8 in a wet atmosphere.[12] It might result from a weakened adsorption strength on the Co_3O_4 surface leading to an improved transfer of surface oxygen species and an improved amount of surface-adsorbed oxygen.[12] A similar catalyst activation might be occurring here when introducing Fe into the catalyst. However, water decreases the activity in CO oxidation,[12] most probably because of the formation of hydroxyl groups that hinder the oxygen transfer.[13–14] This is in line with the evaluation of the conversion profiles in the HT channel during the isothermal dwell period at 300 °C between heating and cooling in Figure S10 under dry conditions (Fig-

ure S10a), activity decrease with time is observed for all catalysts. However, under wet conditions (Figure S10b) the activity remains constant over the whole period even though the conversions for the catalysts Co_3O_4, Co:Fe 64:1, and Co:Fe 32:1 are close to 100%, and conclusions on stability in this regime are not recommended. However, in a comparison between dry and wet in Figure S10c, it becomes obvious that there is a clear difference starting from similar conversions. These results hint at a stabilizing effect of water acting against the catalyst deactivation by most probably preventing the formation of carbonaceous adsorbates. Altogether, this indicates a lower deactivation rate in the wet feed than the dry feed, as also concluded for perovskites.[15]

In the gas phase 2-propanol oxidation, Dissanayake et al. report a high tolerance to water vapor on Co_3O_4, the T_{90} shifts to higher temperatures by 9 °C.[30] In general, lower activity is observed in Co_3O_4-based spinel catalysts in several reactions under wet conditions, e.g., total propane oxidation,[4a] hydrocarbon oxidation,[12] and CO oxidation.[13] The lowered activity in CO oxidation was related to the adsorption of water on Co^{3+} sites, which would be consequently not available for the adsorption of other molecules.[13] Another possible reason is surface coverage with OH groups.[13] Interestingly, on the 110 facet, a CO molecule can additionally be adsorbed on a Co^{3+} with a preadsorbed OH group and still form CO_2.[13]

Based on rate differences at 100 °C, an increase of water's negative effect on the LT channel's activity becomes apparent with Co content in the spinel as seen in Figure 4c, where positive values refer to a detrimental effect of water addition. There is a continuous increase of the negative impact of water in the feed on the activity with the Co content. A similar pattern is observed from individual rates at 100 °C in dry and wet feed (Figure S8b), including the promotional effect of Fe in the Co:Fe 64:1 catalyst. However, an increasingly beneficial effect with Co content in the HT reaction channel is observed during cooling at 200 °C, as shown by the negative values in Figure 4d and the difference in Figure S8c. Higher 2-propanol consumption rates were found for all catalysts under wet conditions except for $CoFe_2O_4$.

In terms of Δ product formation rates shown in Figure 4e, no effect of adding water is observed on the CO_2 formation rate. However, the curve shape of acetone formation is analogous to the 2-propanol consumption, which shows that the higher activity under wet conditions originates from the 2-propanol oxidative dehydration and not from the promotion of the total oxidation. Thus, the yields of acetone as the selective oxidation product are higher in the wet feed. When looking at the difference between dry and wet in the product formation rate ratio at T_{50} during cooling (Figure 4f), this positive effect of the co-feeding of water is observed for all catalysts, and the beneficial effect rises with the Co content. However, two catalysts affected by the Fe promotion showing the highest acetone formation ratio under dry conditions, Co:Fe 64:1 and Co:Fe 32:1, are not as positively affected in the Δ plots as expected from their Co content. The absolute numbers can explain this in Figure S8e showing that by a combination of the two promoting effects of Fe and water, the 100% selectivity is already obtained and cannot be further increased to reveal the full potential.

In summary, the co-feeding of water has diverse impacts on the selective gas phase oxidation of the studied cobalt based spinel catalysts. For all catalysts, the LT activity is negatively affected by the presence of water due to competitive adsorption. However, the promotional effect of low amounts of Fe observed under dry conditions was confirmed when comparing dry and wet feed values. Under wet conditions, the cooling curves are additionally shifted to lower temperatures than at dry conditions, indicating another promoting effect on conversion and selectivity of water in the HT reaction channel or slower catalyst deactivation. This effect was found to scale with the cobalt content at the surface of the catalysts. A likely reason is that the HT channel is more stable under wet conditions, while under isothermal conditions, the LT channel deactivates similarly fast under dry and wet conditions.

Analysis of spent catalysts

The spent catalysts were investigated via TEM, TEM-EDX, XPS, and EELS after the three-run catalytic cycle protocol after storage in air, and the characterization results are shown in Figure 5a for the ratio of Co/(Co + Fe) post-catalysis. There is still a good agreement between XPS and STEM-EDX with the nominal values in the cation's ratio. However, like the as-prepared state, the experimental ratio for $CoFe_2O_4$ differs in the near-surface region compared to the bulk counterpart (obtained from STEM-EDX). No clear change in Co/(Co + Fe) ratio was found both in STEM-EDX and XPS for the as-prepared (ap) and post-catalysis (pc) samples.

However, a notable effect was observed in the contributions of different cobalt oxide species to the overall Co signal in XPS, as seen in the Co signal contributions post-catalysis in Figure 5c. The individual Co 2p spectra after catalysis are shown in Figure S2. For $CoFe_2O_4$, no change is observed in the Co oxidation state distribution, it remains mainly Co^{2+} as expected for an inverse spinel. With increasing Co content, Co:Fe 3:1 and Co:Fe 7:1 still show the normal spinel composition of oxidation states as in Co_3O_4 and therewith no change. However, for Co:Fe 16:1, Co:Fe 32:1, and Co:Fe 64:1, which have 2–7% experimental Fe content, a clear increase of the Co^{2+} content at the near-surface regions after catalysis is observed (Figure 5c). In the post-catalysis spectrum, there is a visible Co^{2+} shake-up peak whereas there is no change in the Co_3O_4 catalyst.[25] The higher content of Co^{2+} species indicates a higher degree of Co reduction during catalysis if Fe is present in low concentrations which might explain the unexpectedly high activity of Co:Fe 32:1 and Co:Fe 64:1 associated with surface Co^{3+} reducibility. From previous work on Co_3O_4, a reduction of the surface to CoO was expected since a reduction was seen in comparing XPS before and after reaction and X-ray absorption spectroscopy.[5c] The prominent change of the Co:Fe 64:1 catalyst after catalysis is also confirmed by local EELS spectroscopy where it is the only catalyst that shows a significant change on Co L_3/L_2 intensity ratio between the as-prepared and post-catalysis state (Fig-

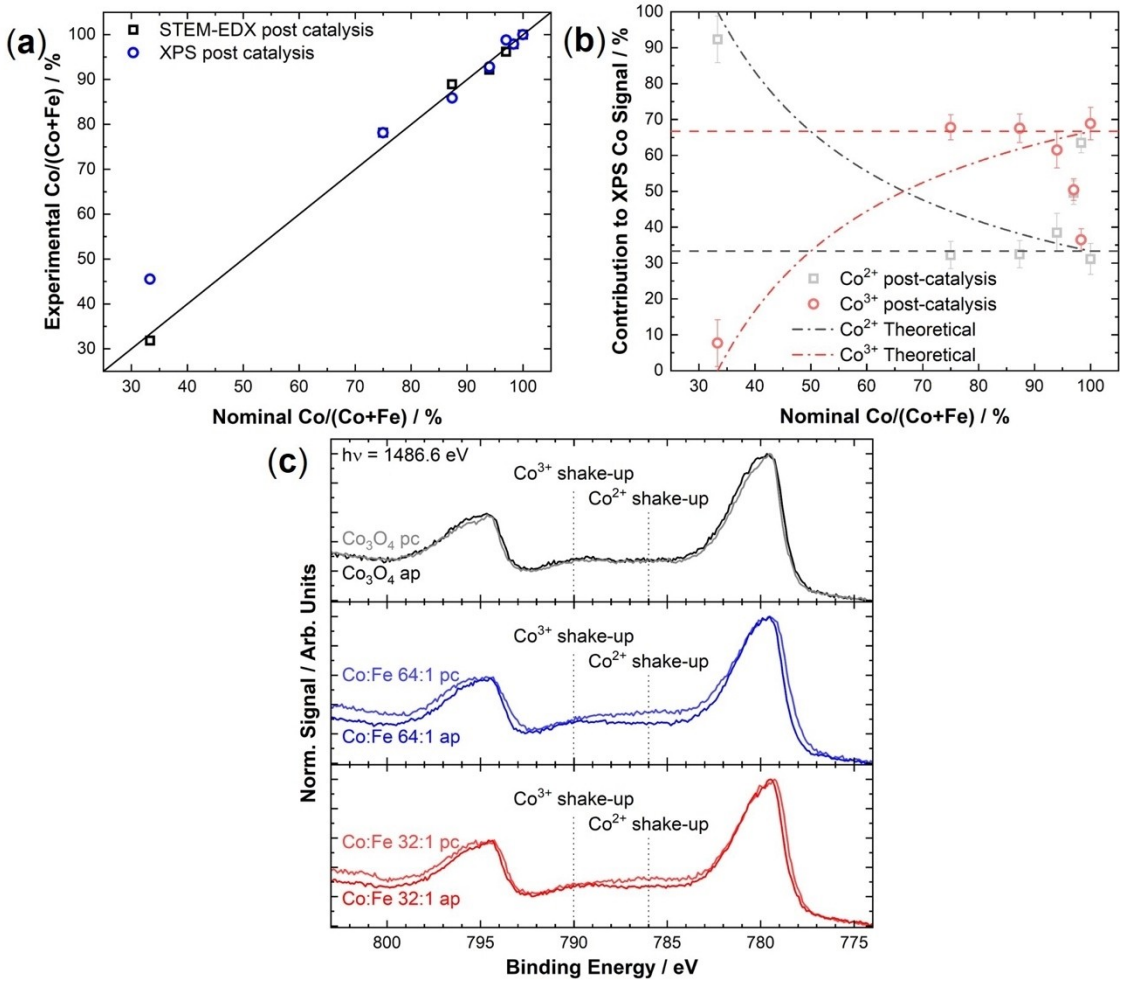

Figure 5. (a) Parity plot of experimental Co/(Co + Fe) ratio derived from STEM-EDX and XPS after catalysis. (b) Differences Δ as-prepared-post catalysis in the experimental Co/(Co + Fe) ratio derived from STEM-EDX and XPS. The dashed horizontal lines indicate the composition of a normal Co_3O_4 spinel with 33.3 % Co^{2+} and 66.7 % Co^{3+}. The hyperbole curves show the Co oxidation states under the assumption that Fe exclusively is present as Fe^{3+}. (c) Co 2p XP spectra of Co_3O_4, Co : Fe 64 : 1, and Co : Fe 32 : 1 in the as-prepared (ap) and post-catalysis (pc) state.

ure S3b). In CO oxidation, Baidya et al. reported activation of Co_3O_4 catalysts with Fe doping synthesized due to an effect of the Fe^{2+}/Fe^{3+} redox couple since TPR showed that the Co^{3+}-O bonding strength is only slightly higher than Fe^{3+}-O, which is in line with our results.[28]

This post-reaction characterization aligns only partially with the previously reported catalyst reduction as the reason for the LT activity loss in the studied particles.[5a–d] Therefore, also the formation of adsorbates on the surface must play an essential role in the deactivation mechanism of the LT channel. TEM images of Co_3O_4 as prepared are shown in Figure 6a and Figure 6b, images post catalysis in Figure 6c and Figure 6d. As seen from comparing the images with lower magnification, the nanowire structure remains intact even after catalysis. The images with higher magnification support this conclusion where indications for surface roughening can be observed as well, which might be due to amorphization and surface reduction, as seen from XPS for catalysts with low Fe contents. These indications are marked with arrows in Figure 6d. The same conclusions are valid for the other catalyst materials, as seen from a comparison of as prepared and post catalysis TEM images for all catalysts in Figure S1.

Altogether, a comparison of XPS and STEM(-EDX) before and after catalysis revealed no significant change in the Co/(Co + Fe) ratio neither in the near-surface region nor in the bulk. However, a reduction of Co^{3+} species to Co^{2+} species is seen from XPS analysis for catalysts with low Fe amounts. The reduction might be accompanied by surface roughening seen in TEM images after catalysis. However, the overall nanowire morphology of the SBA-15 templated catalyst remains undamaged during catalysis. These conclusions need to be taken with care as the ex-situ analysis cannot account for reversible changes. In addition, the change of surface properties due to the contact of the spent catalyst with air during the transfer from the reactor to analytical instruments (TEM and XPS) cannot be excluded. Irrespective of these uncertainties, the comprehensive ex-situ materials analysis suggests that the bulk composition, particle morphology, and structure of the catalysts

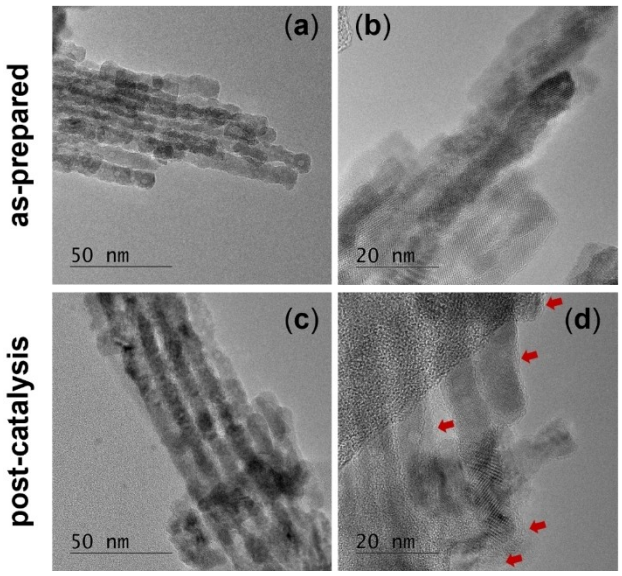

Figure 6. TEM micrographs of Co_3O_4 before catalysis in different magnifications (a) and (b) and after catalysis in different magnifications (c) and (d).

remain largely unchanged throughout catalysis even under wet conditions. This is considered an important prerequisite for the knowledge-based synthesis of $Co_{3-x}Fe_xO_4$ spinels for low-temperature liquid phase oxidation catalysis.

Conclusion

A series of $Co_{3-x}Fe_xO_4$ spinel catalysts was synthesized via the nanocasting route and tested in the gas phase 2-propanol oxidation in dry and wet conditions, i.e., without and with water vapor in the gas feed stream, respectively. The typical spinel catalyst activity behavior of a highly active but non-stable low-temperature and a less active but stable high-temperature channel was found. A beneficial effect of Fe substitution ($\leq$4%) was found under dry and wet conditions to which an increase in the surface area was one contributing factor. Water always affects the activity negatively on the low-temperature channel but has a promoting effect on the high-temperature channel. This promoting effect can be correlated with a lower speed of activity decay during an isothermal experiment. Furthermore, water addition favors the selective oxidation of 2-propanol to acetone. Transmission electron microscopy and energy-dispersive X-ray spectroscopy reveal the structural and chemical stability of the bulk of the nanocasted catalysts throughout catalysis, even under wet conditions. Also, using X-ray photoelectron spectroscopy and electron energy loss spectroscopy, no compositional change during catalysis and no clear correlation between the Co^{2+}/Co^{3+} ratio and Co content in the spinels was found neither before nor after the reaction, except for very low Fe contents. Fe substitution at the doping level, i.e., $\leq$4% showed beneficial effect in the reducibility of the near-surface Co species which correlated with the enhanced surface-area normalized catalytic activities compared to the Co_3O_4.

The comparative characterization and catalytic study on the whole sample series have shown an empirical composition-activity correlation that reliably revealed two promoting effects of Fe substitution at the doping level and water co-feeding. On this basis, forthcoming work can be designed to investigate and understand these phenomena.

Experimental Section

Synthesis and sample preparation

Catalyst materials with controlled mesostructure were prepared by the nanocasting route according to the previous report.[20a] In brief, cobalt and iron precursors (Co:Fe atomic ratio of 100:0, 64:1, 32:1, 16:1, 7:1, 3:1, and 1:2) were prepared by dissolving a stoichiometric amount of $Co(NO_3)_2 \cdot 6H_2O$ and $Fe(NO_3)_3 \cdot 9H_2O$ (Sigma–Aldrich, ACS reagent grade, 99.5% purity) in pure ethanol. The calculated concentration of precursor solution was 0.8 M. The precursor solutions were then impregnated into the pore system of the SBA-15 (that was aged at 100 °C) template by the two-step wet impregnation method (15% total pore filling). For the first impregnation step, a mixture of precursor solution and template was stirred for 2 h. Then the composites were dried in the oven at 50 °C overnight. The first calcination was at 250 °C for 4 h (ramping rate 2 °C min^{-1}). The same impregnation procedure was applied for the second step; however, the final calcination was carried out at 500 °C for 6 h with the intermediate dwell at 250 °C for 4 h (ramping rate 2 °C min^{-1}). As an exception, a slower ramping rate (1 °C min^{-1}) was applied for calcining $CoFe_2O_4$ to avoid the formation of hematite phase (α-Fe_2O_3) in the final product. SBA-15 template was then leached out with a 2 M KOH solution at 70 °C. After four washing cycles and centrifugation in distilled water, the final product was dried in the oven at 80 °C overnight. The materials were pressed and sieved into a sieve fraction of 250–355 μm for catalytic tests and the smaller sieve fraction $<$250 μm was used for the analytics.

Catalyst characterization

X-ray photoelectron spectroscopy (XPS) measurements were performed using a VersaProbe II (Ulvac-Phi, Chanhassen, USA). All the XPS spectra were referenced to the C 1s peak. Casa XPS was used to analyze the spectra. A dual-beam charge neutralization scheme using an electron flood gun with slow-moving Ar^+ ions was employed to counter any charging effects. To identify the Co^{2+} and Co^{3+} ratios, we fitted the Al K_α spectra of the Co 2p by using the peak shapes from a Co^{2+} (CoO) reference from the literature[25a] and a Co^{3+} reference from a $MgCo_2O_4$ material, whose synthesis is published elsewhere.[26] For the set of samples with a non-negligible Fe Auger peak – samples CoFe 7:1, 3:1 and $CoFe_2O_4$ – this peak's position, shape, and intensity were modeled from reference Fe_2O_3 spectra and included in the fitting of the Co 2p spectra. The key fit parameters were the intensities of the reference peaks. To calculate the Co:Fe ratios, we measured the Co and Fe 2p with Mg K_α light to circumvent the Auger-XPS overlapping problem of these two elements occurring with Al K_α radiation.

High-resolution scanning transmission electron microscopy (STEM) studies were carried out on a Jeol JEM 2200 fs microscope (Akishima, Japan) equipped with a probe-side Cs-corrector operated at 200 kV acceleration voltage. Micrographs were taken in

conventional bright field mode. In addition, EDX elemental mappings were acquired with an X-Max 100 detector (Oxford Instruments, Abingdon, United Kingdom). EELS spectra have been acquired using the JEOL omega filter and a Gatan Ultrascan 1000 camera. The FWHM of the zero-loss peak was 1.4 eV. To improve signal-to-noise ratio ten consecutive spectra with 2 s acquisition time have been acquired and summed. The Co L_3/L_2 intensity ratio was determined after power-law background correction and normalization by integration in the respective peak areas using HyperSpy.[31]

Catalytic gas phase 2-propanol oxidation

The measurements were performed in a home-built apparatus consisting of a gas dosing unit (HovaGAS N G6 VOC-S, IAS GmbH, Germany) and a Tube Furnace MTF 10/25/130 (Carbolite Gero, Neuhausen, Germany), which is placed in a heating cabinet Thermocenter TC100 (SalvisLab, Rotkreuz, Switzerland). The reaction mixture, either going through or by-passing the reactor, was analyzed on a downstream dual-carrier gas Fusion Micro GC (Inficon GmbH, Bad Ragaz, Switzerland) equipped with four separation modules (2× Rt-Molsieve 5A, 1× Stabilwax DB, 1× Rt-Q-Bond). 100 mg of the catalyst (sieve fraction of 250–355 μm) was placed in a quartz reactor with an inner diameter of 8 mm.

The test protocol consisted of three runs performed under the same temperature program. Only the reactive gas mixture was changed between the runs. Before each run, temperature-programmed oxidation (TPO) up to 300 °C was performed at a flow rate of 50 mL min^{-1} with an O_2 concentration of 10 % (balanced in N_2), the heating rate was set to 3 °C min^{-1}. The maximum temperature was kept constant for 2 h. Afterward, the temperature was cooled down to 50 °C with a heating rate of 3 °C min^{-1}. The temperature was kept constant for 65 min. During the first 20 min, the remaining O_2 was purged out by N_2 (100 mL min^{-1}). In the last 45 min, the reaction mixture was purged to stabilize the MFC flows. Afterward, the temperature was increased to 300 °C in the reaction mixture with a heating rate of 1 K min^{-1} up and held constant for 1 h. After the isothermal dwell, the temperature was cooled down to 50 °C with a heating rate of 1 K min^{-1} in the reaction mixture. Before starting the next TPO, the temperature was maintained for 10 min under a flow of 100 mL min^{-1} N_2. The reaction mixture consisted of 0.168 % 2-propanol and 0.195 % O_2 balanced in N_2 (dry mixture) for the first two runs and 0.175 % 2-propanol, 0.195 % O_2, and 1.86 % H_2O in N_2 for the third run (wet mixture). The flow rate was kept constant at 100 mL min^{-1}.

Acknowledgements

This work was funded by the Deutsche Forschungsgemeinschaft (DFG, German Research Foundation) – 388390466 – TRR 247 within the projects A1 and C1. MB and SN gratefully acknowledge the financial support from the Mercator Research Center Ruhr (MERCUR, Pe-2018-0034). HT thanks Max Planck Society for the basic funding. We acknowledge support from the Open Access Publication Fund of the University of Duisburg-Essen. Open Access funding was enabled and organized by Projekt DEAL. Open Access funding enabled and organized by Projekt DEAL.

Conflict of Interest

The authors declare no conflict of interest.

Data Availability Statement

The data that support the findings of this study are available from the corresponding author upon reasonable request.

Keywords: 2-propanol · cobalt iron oxide · gas phase · oxidation · spinel phases

[1] a) M. S. Kamal, S. A. Razzak, M. M. Hossain, *Atmos. Environ.* **2016**, *140*, 117–134; b) Z. Zhang, Z. Jiang, W. Shangguan, *Catal. Today* **2016**, *264*, 270–278.
[2] a) G. A. El-Shobaky, M. M. Selim, I. F. Hewaidy, *Surf. Technol.* **1980**, *10*, 55–63; b) S. A. Singh, G. Madras, *Appl. Catal. A* **2015**, *504*, 463–475; c) D. Gu, C. J. Jia, C. Weidenthaler, H. J. Bongard, B. Spliethoff, W. Schmidt, F. Schüth, *J. Am. Chem. Soc.* **2015**, *137*, 11407–11418; d) H. Tüysuz, M. Comotti, F. Schüth, *Chem. Commun. (Camb.)* **2008**, *34*, 4022–4024; e) Y. B. Yu, T. Takei, H. Ohashi, H. He, X. L. Zhang, M. Haruta, *J. Catal.* **2009**, *267*, 121–128.
[3] a) W. Hu, J. Lan, Y. Guo, X.-M. Cao, P. Hu, *ACS Catal.* **2016**, *6*, 5508–5519; b) F. Zasada, J. Grybos, E. Budiyanto, J. Janas, Z. Sojka, *J. Catal.* **2019**, *371*, 224–235; c) F. Zasada, J. Janas, W. Piskorz, M. Gorczynska, Z. Sojka, *ACS Catal.* **2017**, *7*, 2853–2867.
[4] a) W. Zhang, P. Anguita, J. Díez-Ramírez, C. Descorme, J. L. Valverde, A. Giroir-Fendler, *Catalysts* **2020**, *10*; b) G. Chai, W. Zhang, L. F. Liotta, M. Li, Y. Guo, A. Giroir-Fendler, *Appl. Catal. B* **2021**, *298*.
[5] a) T. Falk, S. Anke, H. Hajiyani, S. Saddeler, S. Schulz, R. Pentcheva, B. X. Peng, M. Muhler, *Catal. Sci. Technol.* **2021**, *11*, 7552–7562; b) S. Anke, T. Falk, G. Bendt, I. Sinev, M. Havecker, H. Antoni, I. Zegkinoglou, H. Jeon, A. Knop-Gericke, R. Schlögl, B. Roldan Cuenya, S. Schulz, M. Muhler, *J. Catal.* **2020**, *382*, 57–68; c) S. Anke, G. Bendt, I. Sinev, H. Hajiyani, H. Antoni, I. Zegkinoglou, H. Jeon, R. Pentcheva, B. Roldan Cuenya, S. Schulz, M. Muhler, *ACS Catal.* **2019**, *9*, 5974–5985; d) K. Friedel Ortega, S. Anke, S. Salamon, F. Özcan, J. Heese, C. Andronescu, J. Landers, H. Wende, W. Schuhmann, M. Muhler, T. Lunkenbein, M. Behrens, *Chem. Eur. J.* **2017**, *23*, 12443–12449; e) T. Falk, E. Budiyanto, M. Dreyer, C. Pflieger, D. Waffel, J. Büker, C. Weidenthaler, K. F. Ortega, M. Behrens, H. Tüysüz, M. Muhler, B. Peng, *ChemCatChem* **2021**, *13*, 2942–2951.
[6] M. Dreyer, A. Rabe, E. Budiyanto, K. Friedel Ortega, S. Najafishirtari, H. Tüysüz, M. Behrens, *Catalysts* **2021**, *11*, 1312.
[7] F. Zasada, W. Piskorz, J. Janas, E. Budiyanto, Z. Sojka, *J. Phys. Chem. C* **2017**, *121*, 24128–24143.
[8] Y. Liu, Y. Peng, M. Naschitzki, S. Gewinner, W. Schollkopf, H. Kuhlenbeck, R. Pentcheva, B. Roldan Cuenya, *Angew. Chem. Int. Ed.* **2021**, *60*, 16514–16520.
[9] L. Hu, Q. Peng, Y. Li, *J. Am. Chem. Soc.* **2008**, *130*, 16136–16137.
[10] Q. Ren, S. Mo, R. Peng, Z. Feng, M. Zhang, L. Chen, M. Fu, J. Wu, D. Ye, *J. Mater. Chem. A* **2018**, *6*, 498–509.
[11] L. Lukashuk, N. Yigit, R. Rameshan, E. Kolar, D. Teschner, M. Havecker, A. Knop-Gericke, R. Schlögl, K. Föttinger, G. Rupprechter, *ACS Catal.* **2018**, *8*, 8630–8641.
[12] J. Bae, D. Shin, H. Jeong, C. Choe, Y. Choi, J. W. Han, H. Lee, *ACS Catal.* **2021**, *11*, 11066–11074.
[13] H. F. Wang, R. Kavanagh, Y. L. Guo, Y. Guo, G. Z. Lu, P. Hu, *Angew. Chem. Int. Ed.* **2012**, *51*, 6657–6661; *Angew. Chem.* **2012**, *124*, 6761–6765.
[14] J. Bae, D. Shin, H. Jeong, B.-S. Kim, J. W. Han, H. Lee, *ACS Catal.* **2019**, *9*, 10093–10100.
[15] M. Dreyer, D. Cruz, U. Hagemann, P. Zeller, M. Heidelmann, S. Salamon, J. Landers, A. Rabe, K. F. Ortega, S. Najafishirtari, H. Wende, N. Hartmann, A. Knop-Gericke, R. Schlögl, M. Behrens, *Chem. Eur. J.* **2021**, *27*, 17127–17144.
[16] B. Shi, Z. Zhang, Y. Liu, J. Su, X. Liu, X. Li, J. Wang, M. Zhu, Z. Yang, J. Xu, Y.-F. Han, *J. Catal.* **2020**, *381*, 150–162.
[17] E. Hema, A. Manikandan, M. Gayathri, M. Durka, S. A. Antony, B. R. Venkatraman, *J. Nanosci. Nanotechnol.* **2016**, *16*, 5929–5943.

[18] S. Wójcik, G. Grzybek, P. Stelmachowski, Z. Sojka, A. Kotarba, *Catalysts* **2019**, *10*.
[19] Z. Liu, G. Sun, C. Chen, K. Sun, L. Zeng, L. Yang, Y. Chen, W. Wang, B. Liu, Y. Lu, Y. Pan, Y. Liu, C. Liu, *ACS Catal.* **2020**, *10*, 6803–6809.
[20] a) E. Budiyanto, M. Q. Yu, M. M. Chen, S. DeBeer, O. Rüdiger, H. Tüysüz, *ACS Appl. Energ. Mater.* **2020**, *3*, 8583–8594; b) T. Grewe, X. Deng, H. Tüysüz, *Chem. Mater.* **2014**, *26*, 3162–3168; c) K. Min, M. Hwang, S. E. Shim, D. Lim, S.-H. Baeck, *Chem. Eng. J.* **2021**, *424*.
[21] Y. Peng, H. Hajiyani, R. Pentcheva, *ACS Catal.* **2021**, *11*, 5601–5613.
[22] D. Waffel, E. Budiyanto, T. Porske, J. Büker, T. Falk, Q. Fu, S. Schmidt, H. Tüysüz, M. Muhler, B. X. Peng, *J. Mol. Catal.* **2020**, *498*, 111251.
[23] D. Waffel, B. Alkan, Q. Fu, Y. T. Chen, S. Schmidt, C. Schulz, H. Wiggers, M. Muhler, B. Peng, *ChemPlusChem* **2019**, *84*, 1155–1163.
[24] X. T. Wang, T. Ouyang, L. Wang, J. H. Zhong, T. Ma, Z. Q. Liu, *Angew. Chem. Int. Ed.* **2019**, *58*, 13291–13296; *Angew. Chem.* **2019**, *131*, 13425–13430.
[25] a) M. C. Biesinger, B. P. Payne, A. P. Grosvenor, L. W. M. Lau, A. R. Gerson, R. S. C. Smart, *Appl. Surf. Sci.* **2011**, *257*, 2717–2730; b) T. Mathew, N. R. Shiju, K. Sreekumar, B. S. Rao, C. S. Gopinath, *J. Catal.* **2002**, *210*, 405–417; c) J. Yang, H. Liu, W. N. Martens, R. L. Frost, *J. Phys. Chem. C* **2010**, *114*, 111–119; d) P. N. Anantharamaiah, P. A. Joy, *Phys. Chem. Chem. Phys.* **2016**, *18*, 10516–10527.
[26] A. Rabe, J. Büker, S. Salamon, A. Koul, U. Hagemann, J. Landers, K. Friedel Ortega, B. Peng, M. Muhler, H. Wende, W. Schuhmann, M. Behrens, *Chem. Eur. J.* **2021**, *27*, 17038–17048.
[27] a) Z. L. Wang, J. S. Yin, Y. D. Jiang, *Micron* **2000**, *31*, 571–580; b) Y. Zhao, T. E. Feltes, J. R. Regalbuto, R. J. Meyer, R. F. Klie, *J. Appl. Phys.* **2010**, *108*; c) H. Tan, J. Verbeeck, A. Abakumov, G. Van Tendeloo, *Ultramicroscopy* **2012**, *116*, 24–33; d) Z. Zhang, *Ultramicroscopy* **2007**, *107*, 598–603.
[28] T. Baidya, T. Murayama, P. Bera, O. V. Safonova, P. Steiger, N. K. Katiyar, K. Biswas, M. Haruta, *J. Phys. Chem. C* **2017**, *121*, 15256–15265.
[29] R. Zhang, H. Alamdari, S. Kaliaguine, *Appl. Catal. B* **2007**, *72*, 331–341.
[30] S. Dissanayake, N. Wasalathanthri, A. Shirazi Amin, J. He, S. Poges, D. Rathnayake, S. L. Suib, *Appl. Catal. A* **2020**, *590*.
[31] F. de la Peña, E. Prestat, V. T. Fauske, P. Burdet, J. Lähnemann, T. Furnival, P. Jokubauskas, M. Nord, T. Ostasevicius, K. E. MacArthur, D. N. Johnstone, M. Sarahan, T. Aarholt, J. Taillon, pquinn-dls, V. Migunov, A. Eljarrat, J. Caron, T. Poon, S. Mazzucco, C. Francis, B. Martineau, actions-user, S. Somnath, T. Slater, N. Tappy, M. Walls, N. Cautaerts, F. Winkler, DENSmerijn, v1.6.5 ed., **2021**.

Manuscript received: April 6, 2022
Revised manuscript received: August 3, 2022
Accepted manuscript online: August 4, 2022
Version of record online: August 25, 2022